Article

Not peer-reviewed version

Preparation and Characterization of Light-Colored Polyimide Nanocomposite Films Derived from Fluoro- Containing Semi-Alicyclic Polyimide Matrix and Colloidal Silica with Enhanced High-Temperature Dimensionally Stability

Zhibin He , Xi Ren , Zhenzhong Wang , Zhen Pan , Yuexin Qi , Shujun Han , Haifeng Yu , Jingang Liu *

Posted Date: 20 June 2023

doi: 10.20944/preprints202306.1424.v1

Keywords: polyimide film; optical transparency; coefficient of thermal expansion (CTE); benzanilide; thermal properties

Article

Preparation and Characterization of Light-Colored Polyimide Nanocomposite Films Derived from Fluoro- Containing Semi-Alicyclic Polyimide Matrix and Colloidal Silica with Enhanced High-Temperature Dimensionally Stability

Zhibin He[1] , Xi Ren[2], Zhenzhong Wang[2], Zhen Pan[2], Yuexin Qi[2], Shujun Han[2], Haifeng Yu[1], Jingang Liu[2,*]

[1] School of Material Science and Engineering, Key Laboratory of Polymer Chemistry and Physics of Ministry of Education, Peking University, Beijing, 100871, China; zb.he@stu.pku.edu.cn (Z.H.); yuhaifeng@pku.edu.cn (H.Y.)

[2] Engineering Research Center of Ministry of Education for Geological Carbon Storage and Low Carbon Utilization of Resources, School of Materials Science and Technology, China University of Geosciences, Beijing 100083, China; renxi@email.cugb.edu.cn (X.R.); wzz0808@163.com (Z.W.); 2103210036@email.cugb.edu.cn (Z.P.); qiyuexin1004@163.com (Y.Q.); 15966200097@163.com (S.H.); liujg@cugb.edu.cn (J.L.)

* Correspondence: liujg@cugb.edu.cn (J.L.); Tel.: +86 10 82322972 (J.L.)

Abstract: Light-colored and transparent polyimide (PI) films with good high-temperature dimensional stability are highly desired for advanced optoelectronic applications. However, in practice, the simultaneous achievement of good optical and thermal properties in one PI film is usually difficult due to the inter-conflicting molecular design for the polymers. In the present work, a series of PI-SiO_2 nanocomposite films (ABTFCPI) were developed based on the PI matrix derived from hydrogenated pyromellitic anhydride (HPMDA) and an aromatic diamine containing benzanilide and trifluoromethyl substituents in the structure, 2,2'-bis(trifluoromethyl)-4,4'-bis[4-(4-aminobenzamide)]biphenyl (ABTFMB). The inorganic SiO_2 fillers were incorporated into the nanocomposite films with the form of colloidal nanoparticles dispersed in the good solvent of N,N-dimethylacetamide (DMAc) for the PI matrix. The derived ABTFCPI nanocomposite films showed good film-forming ability, flexible and tough nature, good optical transparency, and good thermal properties with the loading amounts of SiO_2 up to 30 wt% in the system. The ABTFCPI-30 film with the SiO_2 content of 30 wt% in the film showed the optical transmittance of 79.6% at the wavelength of 400 nm (T_{400}) with a thickness of 25 μm, the yellow index (b^*) of 2.15, and the 5% weight loss temperatures ($T_{5\%}$) of 491 °C, which are all comparable to those the pristine ABTFCPI-0 matrix without filler (T_{400}=81.8%; b^*=1.77; $T_{5\%}$=492 °C). Meanwhile, the ABTFCPI-30 film exhibited obviously enhanced high-temperature dimensional stability with the linear coefficients of thermal expansion (CTE) of 25.4×10^{-6}/K in the temperature range of 50 to 250 °C, which is much lower than that of the AMTFCPI-0 film (CTE=32.7×10^{-6}/K).

Keywords: polyimide film; optical transparency; coefficient of thermal expansion (CTE); benzanilide; thermal properties

1. Introduction

Colorless or light-colored polyimide (CPI) films have been widely investigated as high-performance components in modern optoelectronic applications due to the excellent combined thermal, optical, dielectric, and other functionalities [1-3]. However, the common CPI films, either the fluoro-containing or the semi-alicyclic ones usually suffer from the relatively poor high-temperature dimensional stability; that is the high linear coefficients of thermal expansion (CTE)

Preprints (www.preprints.org) | NOT PEER-REVIEWED | Posted: 20 June 2023 doi:10.20944/preprints202306.1424.v1

compared with the commonly used metal or inorganic materials in the current optoelectronic fabrications. For example, the CPI films derived from fluoro-containing dianhydride, 4,4′-hexafluoroisopropylene diphthalic anhydride (6FDA) and fluoro-containing diamine, 2,2′-bis(trifluoromethyl)benzene (TFMB) showed the CTE value of 82×10^{-6}/K [4]. The semi-alicyclic CPI films derived from hydrogenated pyromellitic anhydride (HPMDA) and 4,4′-oxydianiline (ODA) had a CTE value of 57.1×10^{-6}/K [5]. Comparatively, the first generation of silicon-based semiconductor chips showed the CTE value of 3.0×10^{-6}/K [6] and the third generation of silicon carbide (SiC)-based chips showed the CTE value of 4.2×10^{-6}/K [7]. The optical sodalime glass (SLG) and the new-generation of ultrathin glass (UTG) showed the CTE values of 8.9×10^{-6}/K and 7.2×10^{-6}/K, respectively [8]. The mismatch between the CTE values of CPI films and the inorganic components might induce the internal stress during the fabrication of the optoelectronic devices, which might result in the delamination, cracking, warpage and other reliability issues [9]. Thus, it has been becoming one of the most important topics for the improvements of the high-temperature dimensional stability of the CPI films [10-12].

Among various CPI films, the ones based on the alicyclic dianhydrides and aromatic diamines, that is the semi-alicyclic (or semi-aromatic) systems have attracted great attentions in the research and development of high-performance polymers for optoelectronic applications due to the excellent combined thermal, optical, mechanical and dielectric properties and the relatively low cost at the same time [13-16]. Various methodologies based on the molecular design of the functional alicyclic dianhydride or the aromatic diamine monomers have been proposed and carried out to reduce the CTE values of the semi-alicyclic CPI films. For instance, an alicyclic dianhydride monomer having rigid cyclopentanone bis-spironorbornane structure (CpODA) was developed and the derived CPI films showed the reduced CTE values in the range of 17×10^{-6}/K to 57×10^{-6}/K [17]. An alicyclic dianhydride, octahydro-2,3,6,7-anthracenetetracarboxylic dianhydride (OHADA) was recently reported and the CPI films based on the dianhydride monomer showed the CTE value as low as 41.5×10^{-6}/K [18]. An alicyclic dianhydride monomer containing rigid cyclobutane unit, 1,3-dimethyl-1,2,3,4-cyclobutane tetracarboxylic dianhydride (DM-CBDA) was synthesized to develop low-CTE CPI films [19]. The CPI film based on DM-CBDA and TFMB exhibited a CTE value of 28.1×10^{-6}/K, which was much lower than that of the 6FDA-TFMB system (CTE=82×10^{-6}/K). For the diamine monomers, various rigid-rod units have been introduced into the molecular structures of the compounds as so to reduce the CTE values of the derived semi-alicyclic CPI films. Amide (-CONH-) or benzanilide (-Ph-CONH-Ph-) structural units have been proven to be the most effective substituents for achieving this target [20-22]. In our previous work, the aromatic diamines containing amide linkages were developed and the CPI films based on the diamines and the hydrogenated pyromellitic anhydride (HPMDA) showed the reduced CTE values as low as 27.7×10^{-6}/K [23]. However, the optical properties of the derived low-CTE CPI films were deteriorated by the incorporation of the amide components. In view of this defect of the common CPI films derived from the amide-containing diamines, a novel aromatic diamine simultaneously containing rigid-rod benzanilide and highly electronegative trifluoromethyl (–CF_3) units, 2,2'-bis (trifluoromethyl)-4,4'-bis[4-(4-aminobenzamide)]biphenyl (ABTFMB) was designed and developed in Hasegawa's group and was widely used to develop high-performance CPI films [24-26].

Although the semi-alicyclic CPI films derived from alicyclic dianhydride and the ABTFMB or its derivative diamines usually represent the high-performance films with both of high optical transparency and high thermal stability, the CTE values are often required to be further decreased so as to meet the ever-increasing reliability requirements in the optoelectronic fields. Composite seems to be one of the few feasible pathways to achieve this target. Combination with inorganic nanofillers with low thermal expansion characteristics, such as silica (SiO_2), has been proved to be an effective way to further reduce the CTE values of the CPI films [27-30]. However, incorporation of nanoparticles might deteriorate the optical transparency of derived composite films. This requires careful design of the morphology, particle size and surface pretreatment of the nanoparticles. Recently, a special class of silica nanoparticles, colloidal-type silica, has been widely used in the modification of CPI films [29]. In practical applications, colloidal silica nanoparticles were usually dispersed in the good solvent, such as N,N-dimethylacetamide (DMAc) for the CPI film

 doi:10.20944/preprints202306.1424.v1

manufacturing; thus could form uniform dispersion and distribution in the CPI matrix after high-temperature imidization or curing process. The unique physical and chemical properties of the colloidal silica nanoparticles make them achieve a higher loading proportion in the CPI matrix than the traditional nano-silica particles, which can effectively reduce the CTE values of the composite films while maintaining the inherent optical properties of the CPI matrix film to a large extent.

In the current work, a synergistic methodology was used to develop high-performance CPI films with good dimensional stability at elevated temperatures. On one hand, the semi-alicyclic CPI matrix film (ABTFCPI-0) with the low-CTE feature was prepared from HPMDA dianhydride and ABTFMB diamine. On the other hand, colloidal SiO_2 nanoparticles were used as the filler to further reduce the CTE values of the ABTFCPI-0 matrix. Effects of the loading amounts of the colloidal SiO_2 nanoparticles on the properties of the afforded composite films were studied in detail.

2. Materials and Methods

2.1. Materials

Hydrogenated pyromellitic anhydride (HPMDA, purity: 99.7%) and 2,2'-bis(trifluoromethyl)-4,4'-bis[4-(4-aminobenzamide)]biphenyl (ABTFMB, purity: 99.2%) monomers were all prepared and purified in our laboratory. The alicyclic HPMDA dianhydride and the ABTFMB diamine were dried at 180 °C and 80 °C in vacuum for 24 h, respectively prior to use. The colloidal SiO_2 nanoparticles (average diameter: 15 nm; 20 wt% in DMAc) was also prepared in our laboratory by replacing the dispersing agent of pure water of commercially available water-based colloidal SiO_2 (VPS NE20, Evonik Industrial Co., Ltd., Germany) with ultra-dry DMAc solvent (InnoChem Science & Technology Co., Ltd., Beijing, China). The ultra-dry γ-butyrolactone (GBL) solvent with the water contents below 50 ppm (InnoChem Science & Technology Co., Ltd., Beijing, China) and the other commercially available reagents were used as received.

2.2. Characterization methods

The number average molecular weight (M_n) and weight average molecular weight (M_w) of the ABTFCPI-0 resin were measured using a gel permeation chromatography (GPC) system (Shimadzu, Kyoto, Japan) with HPLC grade N-methyl-2-pyrrolidone (NMP) as the mobile phase. Fourier transform infrared (FTIR) spectra of the CPI films were recorded on an Iraffinity-1S FT-IR spectrometer (Shimadzu, Kyoto, Japan). Hydrogen nuclear magnetic resonance (^{1}H-NMR) of the ABTFCPI-0 resin was measured on an AV 400 spectrometer (Ettlingen, Germany) operating at 400 MHz in deuterated dimethyl sulfoxide (DMSO-d_6). Ultraviolet-visible (UV-Vis) spectra of the CPI films were recorded on a Hitachi U-3210 spectrophotometer (Tokyo, Japan) at room temperature. Wide-angle X-ray diffractions (XRD) of the CPI films were performed on a Rigaku D/max-2500 X-ray diffractometer (Tokyo, Japan) with Cu-Kα1 radiation, operated at 40 kV and 200 mA. X-ray photoelectron spectroscopy (XPS) was measured with an ESCALab220i-XL electron spectrometer (Thermo Fisher Scientific, Massachusetts, USA) using 300 W of MgKα radiation. Yellow index (YI) values of the CPI films were measured using an X-rite color i7 spectrophotometer (Grand Rapids, Michigan, USA) with PI samples at a thickness of 50 μm. The color parameters were recorded according to a CIE Lab equation. L^* is the lightness, where 100 means white and 0 implies black. A positive a^* means a red color, and a negative one indicates a green color. A positive b^* means a yellow color, and a negative one indicates a blue color. Thermogravimetric analyses (TGA) of the CPI films were recorded on a TA-Q series thermal analysis system (New Castle, Delaware, USA) at a heating rate of 20 °C/min in nitrogen. Dynamic mechanical analysis (DMA) was recorded on a TA-Q800 thermal analysis system (New Castle, Delaware, USA) at a heating rate of 5 °C /min and a frequency of 1Hz in nitrogen. Thermo-mechanical analyses (TMA) of the CPI films were performed on a TMA402F3 thermal analysis system (NETZSCH, Selb, Germany) with a heating rate of 5 °C/min in nitrogen. The CTE values of the CPI films were recorded in the range of 50~250 °C.

2.3. CPI resin synthesis and the film preparation

Preprints (www.preprints.org) | NOT PEER-REVIEWED | Posted: 20 June 2023 doi:10.20944/preprints202306.1424.v1

The ABTFCPI-0 matrix resin was synthesized via a well-established one-stage high-temperature polycondensation procedure in the literature. As a demonstration, into a 1000 mL four-necked glass vessel equipped with a mechanical stirrer, an oil bath, Dean-Stark trap and a nitrogen inlet was added ABTFMB (55.8470 g, 100 mmol) and GBL (200.0 g). Nitrogen was passed though the diamine solution in the flask and a transparent ABTFMB solution was obtained after stirring at room temperature for 30 min. HPMDA (22.4170 g, 100 mmol) was then added to the ABTFMB solution and GBL (34.8 g) was added to make the solid content of the polymerization system to be 25 wt%. The reaction system was stirred for 3 h and the solution temperature slightly increased. Then, the imidization catalyst of isoquinoline (0.5 g) and the water azeotropic agent of toluene (200 mL) were added. The reaction system was heated via the oil bath and the toluene-water azeotrope appeared in the system when the temperature reached 130~135 °C. The water by-product was continuously distilled out of the system via the azeotrope until no droplet was observed in the Dean-Stark trap (~6 h). The residual toluene was distilled out of the reaction system and the temperature gradually increased to 180 °C. The polymerization temperature was maintained for 6 h and then cooled to room temperature. The obtained viscous solution with the pale-brown color was then poured into aqueous ethanol solution (1000 mL, ethanol:water=70:30, volume ratio). The off-white silky resin continuously precipitated into the ethanol solution. The obtained ABTFCPI-0 resin was immersed into the ethanol solution for 48 h and then collected and dried at 100 °C in vacuum for 24 h. Yield: 71.9 g (96.3 %). Numeric average molecular weight (M_n): 1.11×10^5 g/mol; weight average molecular weight (M_w): 2.08×10^5 g/mol; polydispersity index (PDI): 1.87. ^{1}H-NMR (DMSO-d_6, ppm): 10.77 (s, 2H), 8.37-8.08 (m, 8H), 7.57-7.40 (m, 6H), 3.33-3.30 (m, 4H), and 2.28-2.09 (m, 4H).

The ABTFCPI-0 resin was re-dissolved in ultra-dry DMAc solvent at room temperature according to the formulas shown in Table 1. Then, the colloidal silica ($cSiO_2$)/DMAc solution was dispersed into the ABTFCPI-0/DMAc solution under supersonic treatment for 1 h. The total solid contents of the CPI solutions were controlled to be 20 wt%. The weight percent of the colloidal silica nanoparticles in the CPI films increased from 0 (ABTFCPI-0) to 30 wt% (ABTFCPI-30). Taking ABTFCPI-30 as an example, ABTFCPI-0 resin (14.0 g) was added into DMAc (56.0 g) in a 250 mL three-necked flask equipped with a mechanical stirrer. The solution was stirred overnight until a homogeneous and transparent varnish was obtained. The varnish was then purified by filtration through a 0.45 μm Teflon syringe filter. The purified solution was mechanically blended with the colloidal silica dispersion (30.0 g) at room temperature for 2 h and then further treated with a supersonic oscillator for another 1 h. The obtained varnish was coated on a clean borosilicate glass and thermally dried in a clean oven with the heating procedure of 80 °C/3 h, 150 °C/1 h, 180 °C/1 h, 200 °C/1 h, and 250 °C/1 h. After the thermal treatment, the glass substrate was cooled to room temperature and immersed into the deionized water. Free-standing ABTFCPI-30 film automatically peeled off the substrate, which was further dried in vacuum at 120 °C for 24h. ABTFCPI-0 films with various thicknesses in the range of 10-100 μm were separately prepared for the following characterization. The other composite films, including ABTFCPI-5, ABTFCPI-10, ABTFCPI-15, ABTFCPI-20, and ABTFCPI-25 were prepared according to a similar procedure as mentioned above. For the preparation of the pure ABTFCPI-0 film, no colloidal silica nanoparticles were added.

Table 1. Formulas for the preparation of ABTFCPI nanocomposite films.

samples	ABTFCPI-0, DMAc (g, g)	$cSiO_2$ (20 wt% in DMAc, g)	M_{SiO2}/M_{total} (wt%)
ABTFCPI-0	20.0, 80.0	0	0
ABTFCPI-5	19.0, 76.0	5.0	5
ABTFCPI-10	18.0, 72.0	10.0	10
ABTFCPI-15	17.0, 68.0	15.0	15
ABTFCPI-20	16.0, 64.0	20.0	20
ABTFCPI-25	15.0, 60.0	25.0	25
ABTFCPI-30	14.0, 56.0	30.0	30
ABTFCPI-35	13.0, 52.0	35.0	35

Preprints (www.preprints.org) | NOT PEER-REVIEWED | Posted: 20 June 2023 doi:10.20944/preprints202306.1424.v1

3. Results and discussion

3.1. CPI resin synthesis and film preparation

One pure CPI (ABTFCPI-0) and seven CPI nanocomposite films (ABTFCPI-5~ABTFCPI-35) were prepared, respectively based on the ABTFCPI-0 matrix resin, as shown in **Figure 1**. The resin was soluble in the polycondensation system despite the existence of the rigid-rod benzanilide units in the diamine moiety. The non-conjugated molecular structure feature in the HPMDA dianhydride moiety endowed the derived resin good solubility in the reaction media. The resin was soluble in both of polar aprotic solvents, such as N,N–dimethylformamide (DMF), DMAc, NMP, dimethyl sulfoxide (DMSO) and common polar solvents, such as cyclopentanone, chloroform, and so on at the solid content of 10 wt%.

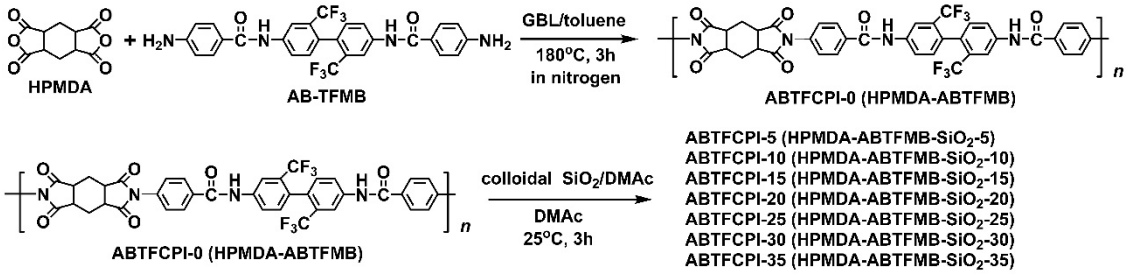

Figure 1. Preparation of semi-alicyclic amide-bridged PIs.

The good solubility of the ABTFCPI-0 resin in organic solvents made it possible to confirm the structure by ^{1}H-NMR measurements, as illustrated in **Figure 2**. In the figure, the characteristic absorptions of hydrogen protons in the amide (–CONH–) units, in the aromatic rings (H_1~H_5), and in the alicyclic rings (H_a, H_b, and $H_{b'}$) could be clearly assigned. As expected, the amide proton exhibited the absorption at the chemical shift of 10.77 ppm, which was at the farthest downfield in the spectra. This is due to the strong electron-withdrawing carbonyl group. Similarly, the absorption of H_3 appeared at the second farthest downfield in the spectra due to the ortho-substituted –CF_3 groups with the high electronegativity. Contrarily, the absorptions of the cyclohexane protons were present at the upfield in the spectra due to the electron-donating features of the alicyclic rings. This is consistent with the structural features of the ABTFCPI-0 resin.

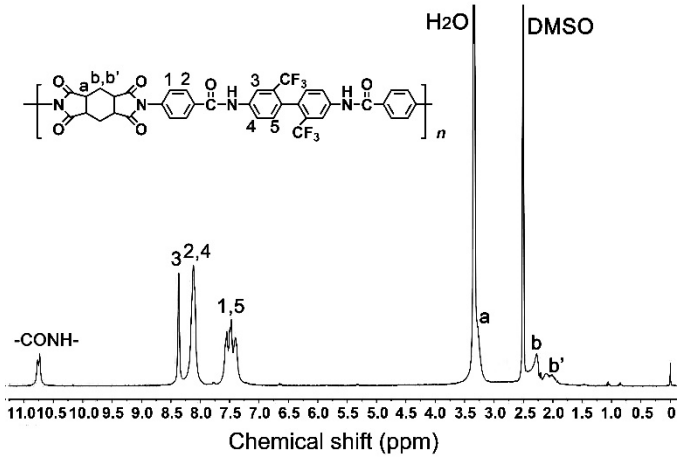

Figure 2. ^{1}H-NMR spectrum of ABTFCPI-0 resin.

The pure ABTFCPI-0 film and the ABTFCPI-SiO_2 nanocomposite films (ABTFCPI-5~ABTFCPI-35) were prepared according to the procedure shown in **Figure 3**. All the films showed flexible and tough characters except ABTFCPI-35, which was a bit brittle and couldn't be folded like the other counterparts. The good flexibility of the nanocomposite films was on one hand due to the merits of the ABTFCPI-0 matrix and on the other hand owing to the good dispersion and distribution of the

Preprints (www.preprints.org) | NOT PEER-REVIEWED | Posted: 20 June 2023 doi:10.20944/preprints202306.1424.v1

SiO_2 nanoparticles. The ABTFCPI-0 resin showed the numerical average molecular weight (M_n) of 1.11×10^5 g/mol, the weight average molecular weight (M_w) of 2.08×10^5 g/mol, and the polydispersity index (PDI) of 1.87. The high molecular weights of the resin could endow the derived films good strength and toughness. As for the colloidal silica nanoparticles, they could be uniformly dispersed into the pristine ABTFCPI-0 matrix due to the specific physical and chemical features of the fillers. Few aggregations were observed for the nanoparticles in the composite films, as could be evidenced by the clear and transparent appearance of the composite solutions and films shown in Figure 3. Even the loading amounts of the SiO_2 fillers reached 35 wt%, the composite films still maintain good optical transparency.

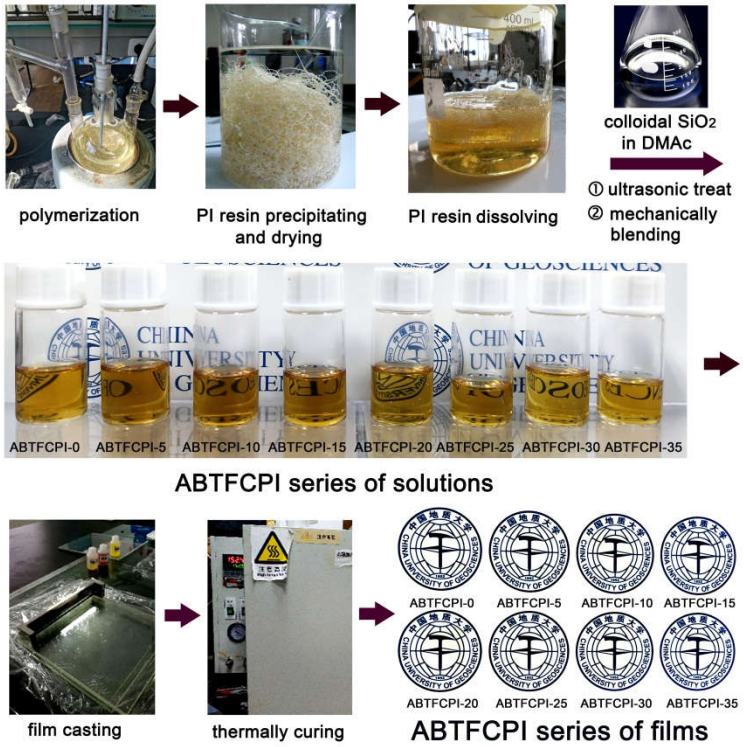

Figure 3. Fabrication diagram of ABTFCPI-0 and ABTFCPI nanocomposite films.

The successful dispersion of the SiO_2 nano-fillers in the composite films could further be proven by the XRD and XPS measurements. As could be seen from the XRD plots of the polymer films shown in **Figure 4**, either the pristine ABTFCPI-0 film or the nanocomposite films exhibited amorphous nature although the SiO_2 nanoparticles showed somewhat crystalline characters. This is mainly ascribed to the non-conjugated feature of the cyclohexane rings in the dianhydride moiety, which efficiently prohibited the formation of crystalline regions in the polymers. In addition, it could be deduced from the full width at half maxima (FWHM) values of the samples labeled in the figure that the FWHM values increased with the increasing SiO_2 contents in the films. This indicates that the partially ordered molecular packing structures in the films were gradually destroyed with the increasing contents of the SiO_2. On the other hand, it also indicates that with the increase of the SiO_2 fillers, some interactions between the SiO_2 particles and the ABTFCPI-0 matrix occurred, causing a lower crystallinity in the films. The loose molecular packing in the nanocomposite films was beneficial for the penetration of visible light and endowed the films good optical transparency.

Figure 5 depicts the XPS plots of the ABTFCPI films. All the samples showed clear absorptions of common elements, including the F1s at the binding energy of 688 eV, O1s at 532 eV, N1s at 400 eV, and C1s at 284 eV. However, only the composite films showed the absorptions of Si2p in the range of 100~153 eV, as could be seen from Figure 5a. In addition, from the expanded binding energy ranged from 99 to 107 eV (Figure 5b), one can observe that the absorption of Si2p increased with the increasing contents of the SiO_2 fillers in the polymers. This is in good agreement with the composition characters of the nanocomposite films.

Preprints (www.preprints.org) | NOT PEER-REVIEWED | Posted: 20 June 2023 doi:10.20944/preprints202306.1424.v1

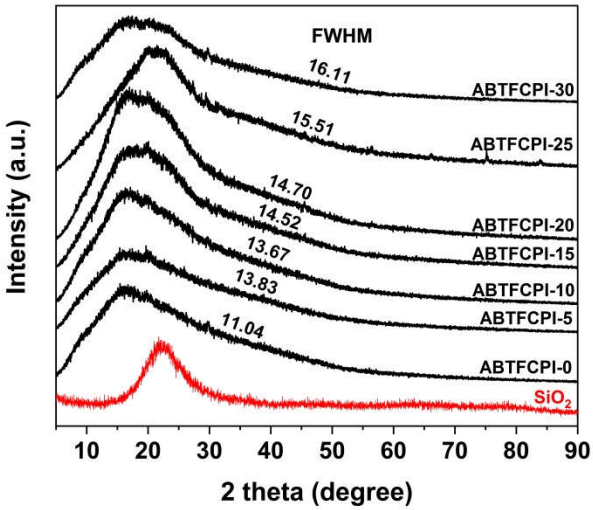

Figure 4. XRD patterns of ABTFCPI films.

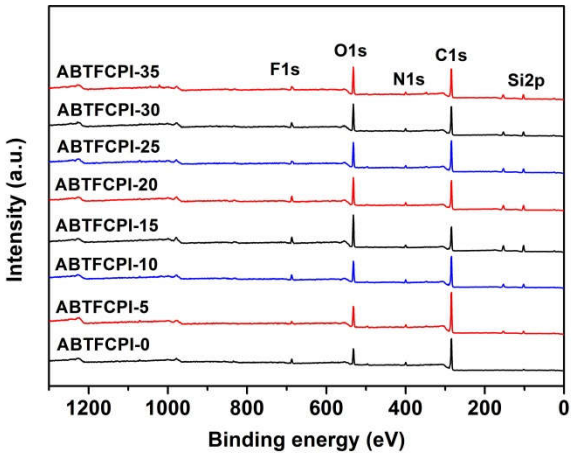

(a)

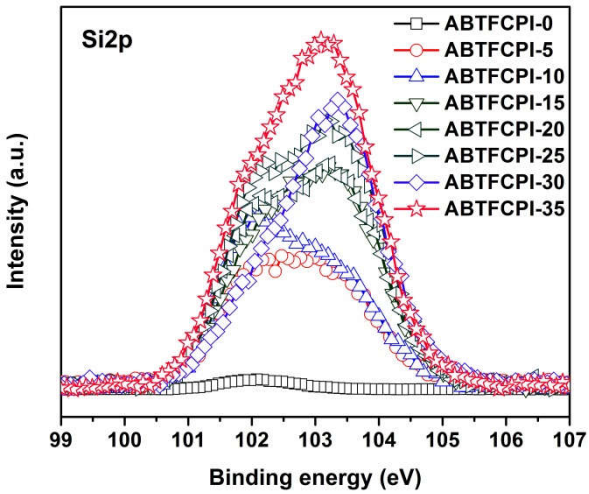

(b)

Figure 5. XPS plots of ABTFCPI films. (a) all-element plots; (b) Si2p plots.

After confirming the successful incorporation of SiO_2 nanoparticles into the ABTFCPI-0 matrix, the chemical structures of the polymers were identified by the FTIR measurements. **Figure 6** shows

Preprints (www.preprints.org) | NOT PEER-REVIEWED | Posted: 20 June 2023 doi:10.20944/preprints202306.1424.v1

the FTIR spectra of the ABTFCPI films. The spectra revealed the characteristic absorptions peaks of the imide rings for all the polymers, including the asymmetrical and symmetrical carbonyl stretching vibrations at 1785 cm^{-1} and 1710 cm^{-1} and the C–N at 1381 cm^{-1}. In addition, the phenyl C=C stretching vibrations at 1504 cm^{-1} and the amide (–CONH–) carbonyl stretching vibrations at 1670 cm^{-1} were also observed. The Si–O stretching vibrations at 1049 cm^{-1} were only detected for the composite films, indicating the incorporation of the silica fillers. At last, the C–H stretching vibrations in cyclohexane units at 3000~2900 cm^{-1} were also detected.

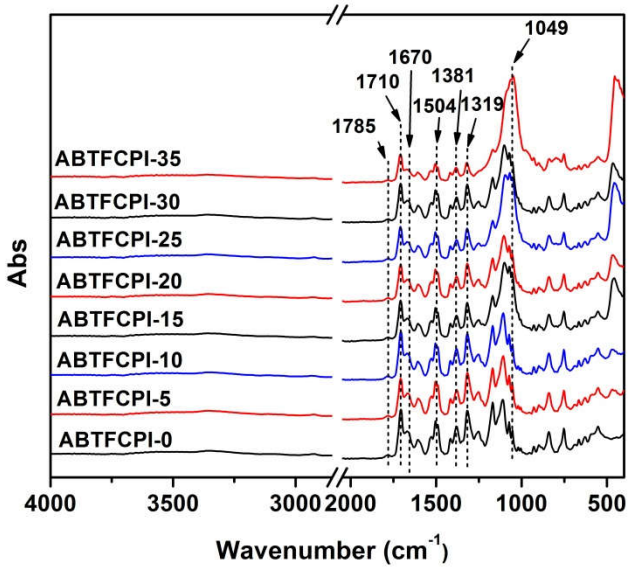

Figure 6. FTIR spectra of ABTFCPI films.

3.2. Optical properties

Deterioration of the optical properties of the nanocomposite films due to the aggregation of the incorporated nanoparticles has been becoming one of the most concerned issues in the development of high-performance organic/inorganic composite optical films. After all, maintaining the intrinsic optical transparency and low color parameters of the pristine optical films is always the prerequisite in practical applications. Nano-sized silica fillers have been one of the most important functional fillers to compensate the defects of the common polymeric films, such as the relatively poor dimensional stability at elevated temperatures, the low modulus, the low flame retardancy, and the so on. However, the common silica nanoparticle usually aggregated in the optical film matrixes, especially at the high loading amounts. Thus, special surface treatments and additional dispersion treatments are usually required during the fabrication of the nanocomposite films. Even by these methodologies, the loading proportions of the nano-fillers in the final composite films were usually controlled at a relatively low level (<10 wt%). By contrast, colloidal silica (cSiO_2) or silica sols nanoparticles dispersed in water or organic solvents exhibited good dispersion and distribution in the polymer films. Usually, the functionalization of the SiO_2 surface introduces organic groups that make the colloidal SiO_2 particles surface-active and sterically stable. The particles are amorphous, but the particle surface is composed of silanol groups, which is the hydroxyl group connected to the silicon atom. The increased surface activity of SiO_2 particles enables them to act as an emulsifier. In general, silica sols are an aqueous suspension of colloidal SiO_2 particles. In order to endow the silica sols good compatibility with the ABTFCPI-0 matrix, the commercially available aqueous cSiO_2 dispersion was modified by solvent replacement in the current work, in which the water was replaced by DMAc.

Figure 7 and **Figure 8** show the UV-Vis spectra and the 3D CIE Lab optical parameters of the ABTFCPI films and the detailed data are summarized in **Table 2**. As expected, both of the pristine ABTFCPI-0 and the nanocomposite films showed good optical transparency and low yellow indices. Incorporation of the cSiO_2 nanoparticles didn't deteriorate the optical properties of the derived films

Preprints (www.preprints.org) | NOT PEER-REVIEWED | Posted: 20 June 2023 doi:10.20944/preprints202306.1424.v1

even at the high loading contents of 35 wt%. As shown in the figures and Table 2, the optical transmittance of the ABTFCPI films at the wavelength of 400 nm (T_{400}) showed a trend of increasing first and then decreasing with the incorporation of silica nanoparticles. For example, the T_{400} value of the pristine ABTFCPI-0 film was 81.8%, while the ABTFCPI-5 film containing the 5 wt% of silica fillers showed the value of 82.0%. With the further increase of the nanoparticles, the T_{400} values of the nanocomposite film gradually decreased, and the T_{400} value of the ABTFCPI-35 film was as low as 77.2%. This shows that although the introduction of silica nanofillers maintained the intrinsict optical transparency of the nanocomposite films, a certain degree of aggregation still occurred at the high loading contents of the nanoparticles, making the optical transmittance of the films slightly deteriorated. As can be seen from the CIE Lab parameters shown in Figure 8, the brightness (L^*) values of the nanocomposite films slightly increased with the increasing of the silica fillers, but the yellow indices (b^*) also increased, showing a trend of yellowing for the films. The haze values of the nanocomposite films remained at a relatively stable level. It can be concluded seen that the nanocomposite films could maintain the inherent optical characteristics of the pristine ABTFCPI-0 film when the silica contents were below 30 wt%.

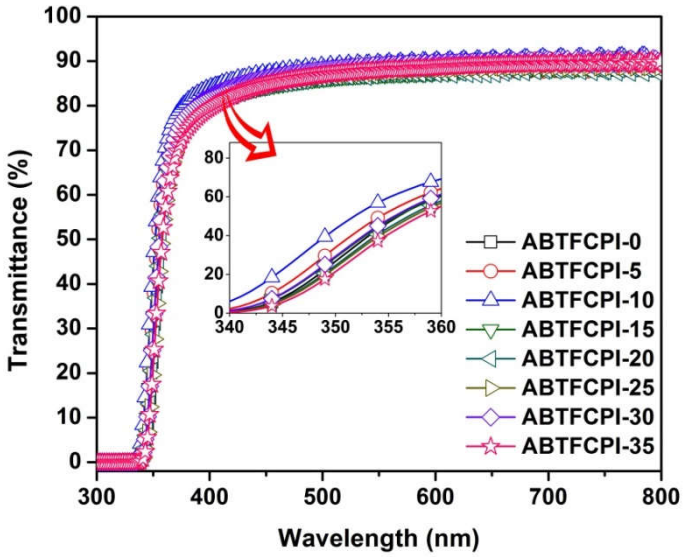

Figure 7. UV-Vis spectra of ABTFCPI films.

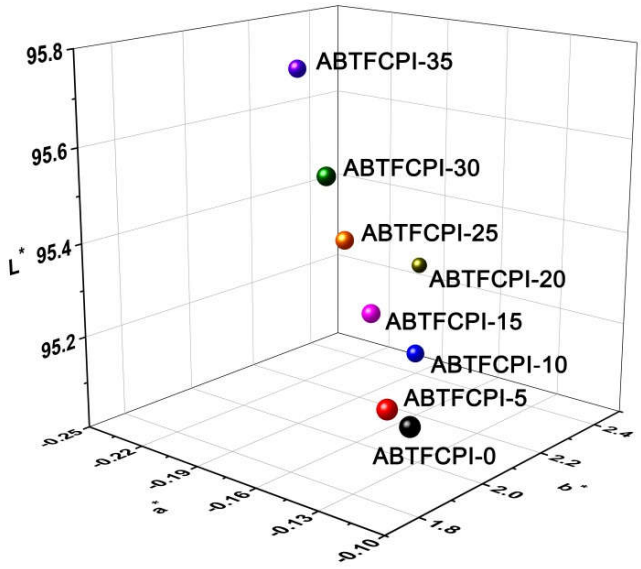

Figure 8. CIE Lab color parameters of ABTFCPI films.

Preprints (www.preprints.org) | NOT PEER-REVIEWED | Posted: 20 June 2023 doi:10.20944/preprints202306.1424.v1

Table 2. Optical and thermal properties of ABTFCPI films.

PI	Optical properties [a]						Thermal properties [b]			
	(nm)	T_{400} (%)	L^*	a^*	b^*	haze (%)	T_g (°C)	$T_{5\%}$ (°C)	R_{w750} (%)	CTE (×10^{-6}/K)
ABTFCPI-0	338	81.8	95.19	-0.10	1.77	0.25	390.3	492	47.8	32.7
ABTFCPI-5	336	82.0	95.21	-0.11	1.77	0.66	389.9	488	47.7	28.9
ABTFCPI-10	338	80.3	95.08	-0.18	2.33	0.24	387.2	491	48.7	28.1
ABTFCPI-15	337	80.4	95.24	-0.17	2.11	0.27	391.4	494	56.9	25.8
ABTFCPI-20	338	80.1	95.10	-0.25	2.82	0.54	389.2	492	53.5	27.5
ABTFCPI-25	333	83.8	95.54	-0.18	2.03	0.13	388.5	493	60.6	28.3
ABTFCPI-30	338	79.6	95.37	-0.19	2.15	0.50	386.1	491	56.4	25.4
ABTFCPI-35	339	77.2	95.70	-0.23	2.24	0.42	388.3	494	64.7	ND

[a] λ: Cutoff wavelength; T_{400}: Transmittance at the wavelength of 400 nm with a thickness of 50 μm; L^*, a^*, b^*, see Measurements part. [b] T_g: Glass transition temperatures defined as the peak temperatures of loss modulus in DMA measurements; $T_{5\%}$: Temperatures at 5% weight loss; R_{w700}: Residual weight ratio at 750 °C in nitrogen; CTE: linear coefficient of thermal expansion in the range of 50~250 °C. ND: not detected.

3.3. Thermal properties

The thermal properties of the ABTFCPI films, including the 5% weight loss temperatures ($T_{5\%}$), the residual weight ratios at 750 °C (R_{w750}) the glass transition temperatures (T_g), and the linear coefficients of thermal expansion (CTE) were investigated by TGA, DMA, and TMA measurements, respectively. The thermal properties data are tabulated in Table 2.

First, the TGA and the derivative TG (DTG) plots of the samples are illustrated in **Figure 9.** All the ABTFCPI films showed good thermal stability before 450 °C. The films began to thermally decompose around 500 °C and revealed the similar $T_{5\%}$ values in the range of 488~494 °C. According to the DTG plots, the most rapid thermal decomposition occurred in the range of 500~525 °C. At 750 °C, the samples maintained 47.8~64.7 % of their original weights. From the above thermal data, it can be deduced that incorporation of the $cSiO_2$ nanoparticles had little effects on the initial thermal decomposition behaviors; however could efficiently increase the R_{w750} values of the composite films. This is mainly ascribed to the high thermal stability of the inorganic $cSiO_2$ fillers at elevated temperatures.

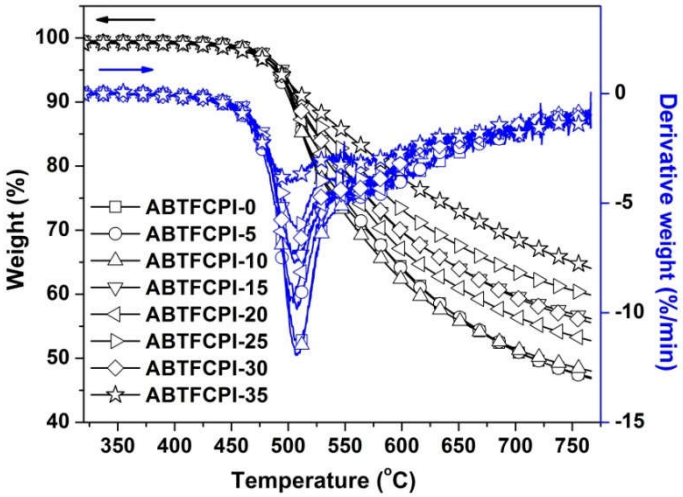

Figure 9. TGA and DTG curves of PI films in nitrogen.

Secondly, the T_g values of the ABTFCPI films were determined by the DMA measurements, as shown in **Figure 10.** It can be seen that, the ABTFCPI films maintained most of the initial storage and loss modulus up to 350 °C, after which the modulus dramatically decreased. As for the tanδ plots, the inflection point temperatures of the samples were not detected before 400 °C, which is the upper

Preprints (www.preprints.org) | NOT PEER-REVIEWED | Posted: 20 June 2023 doi:10.20944/preprints202306.1424.v1

limitation of the DMA equipment in the current work. The peak temperatures of the loss modulus plots were recognized as the T_g values of the films. According to this definition, the ABTFCPI-0 film showed the T_g of 390.3 °C and the nanocomposite films exhibited similar T_g values, indicating the little effects of the $cSiO_2$ nanoparticles on the glass transition behaviors of the films. This also verified the thermal stability of inorganic silica fillers at elevated temperatures. The high-T_g features of the current ABTFCPI films were mainly attributed to the rigid-rod benzanilide and biphenylene units in the polymers. Strong chemical bonds, such as hydrogen bonds might form among the ABTFCPI molecular chains, which efficiently prohibited the free motions of the molecular segments in the polymers at elevated temperatures.

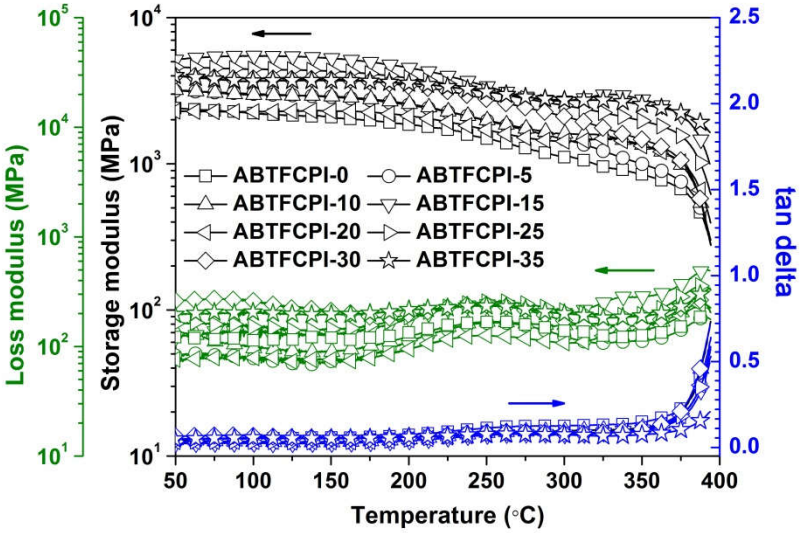

Figure 10. DMA curves of PI films.

At last, the high-temperature dimensional stabilities of the ABTFCPI films were evaluated by the TMA measurements. **Figure 11** depicts the TMA curves of the ABTFCPI films together with the expanded image in the temperature range of 360~420 °C. The pristine ABTFCPI-0 film showed a CTE value of 32.7×10^{-6}/K in the range of 50~250 °C (Table 2). This value ranked lower in all of the semi-alicyclic PI films, which are also the effects of the rigid-rod benzanilide and biphenylene units in the polymers. Incorporation of the rigid amide or benzanilide linkages have been widely used to develop CPI films with the low-CTE features. When incorporating with the $cSiO_2$ nanoparticles, the CTE values of the CPI films further decreased. For example, ABTFCPI-30 film showed a CTE value of 25.4×10^{-6}/K, which was 22.3% lower than that of the pristine ABTFCPI film. In addition, it can be seen from the inserted picture that the ABTFCPI-25 and ABTFCPI-30 films with the higher loading contents of $cSiO_2$ fillers showed much lower dimensional expansion at elevated temperatures. Undoubtedly, the inorganic $cSiO_2$ fillers efficiently increased the dimensional stability of the nanocomposite films. On one hand, this might be contributed to the good dispersion and distribution of the $cSiO_2$ nanoparticles. On the other hand, the possible strong interactions between the hydroxyl (–OH) groups on the surface of the silica fillers and the amide bond (–CONH–) in the molecular structure of the ABTFCPI matrix film may also contribute to the reduction of CTE.

Preprints (www.preprints.org) | NOT PEER-REVIEWED | Posted: 20 June 2023 doi:10.20944/preprints202306.1424.v1

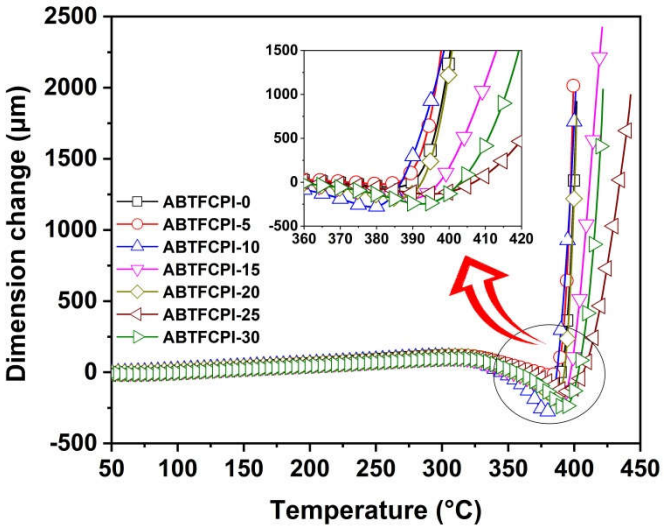

Figure 13. TMA curves of PI films.

4. Conclusions

Semi-alicyclic CPI-SiO_2 nanocomposite films with enhanced high-temperature dimensional stabilities were designed and prepared by incorporation of the colloidal silica nanoparticles into a CPI matrix film containing rigid-rod benzanilide and trifluoromethyl-substituted biphenylene units in the structure. The low-CTE features for both of the matrix film and the fillers endowed the derived nanocomposite films excellent combined properties. As for the optical properties, incorporation of the silica fillers didn't severely deteriorate the optical transparency and color parameters of the derived nanocomposite films. As for the thermal properties, introduction of the silica particles efficiently reduced the CTE values of the final films while maintaining the high T_g and high initial decomposition temperatures. ABTFCPI-30 film showed the best properties, including a T_{400} value of 79.6%, a b^* value of 2.15, a haze value of 0.50, a $T_{5\%}$ value of 491 °C, a T_g value of 386.1 °C, and a CTE value of 25.4×10^{-6}/K, which making it a good candidate for advanced optical applications.

Author Contributions: Conceptualization, J.G.L. and H.F.Y.; Methodology, J.G.L. and H.F.Y.; Investigation, Z.B.H., X.R., and Z.Z.W., Data curation, Z.B.H., X.R., Z.P., Y.X.Q. and S.J.H.; Writing—original draft preparation, Z.B.H.; Writing—review and editing, J.G.L.; Supervision, J.G.L. and H.F.Y.; Funding acquisition, J.G.L.

Funding: This work was supported by Shenzhen Science and Technology Program (No. JSGG20210629144539012) and the Shandong Key Research and Development Program (No. 2019JZZY020235).

Institutional Review Board Statement: Not applicable.

Informed Consent Statement: Informed consent was obtained from all subjects involved in the study.

Data Availability Statement: Data are contained within the article.

Conflicts of Interest: The authors declare no conflict of interest.

References

1. Su, C., Liu, P., Yue, J., Huan, H., Yang, Z., Yang, K., Guo, H., Zhao, J. High-transparency and colorless polyimide film prepared by inhibiting the formation of chromophores. Polymers **2022**, 14(19): 4242.
2. Feng, J., Wang, Y., Qin, X., Lv, Y., Huang, Y., Yang, Q., Li, G., Kong, M. Revealing molecular mechanisms of colorless transparent polyimide films under photo-oxidation. Polym. Degrad. Stab. **2023**, 210, 110294.
3. Jeon, H., Kwac, L.K., Kim, H.G., Chang, J.H. Comparison of properties of colorless and transparent polyimide films using various diamine monomers. Rev. Adv. Mater. Sci. **2022**, 61, 394–404.
4. Matsuura, T., Hasuda, Y., Nishi, S., Yamada, N. Polyimide derived from 2,2-bis(trifluoromethyl)-4,4-diaminobiphenyl. 1. Synthesis and characterization of polyimides prepared with 2,2-bis(3,4-dicarboxyphenyl)hexafluoropropane dianhydride or pyromellitic dianhydride. Macromolecules, **1991**, 24, 5001–5005.

5. Hasegawa, M., Hirano, D., Fujii, M., Haga, M., Takezawa, E., Yamaguchi, S., Ishikawa, A., Kagayama, T. Solution-processable colorless polyimides derived from hydrogenated pyromellitic dianhydride with controlled steric structure. J. Polym. Sci., Part A: Polym. Chem. 2013, 51, 575–592.
6. Sha, C.H., Lee, C.C. Low-temperature solid-state silver bonding of silicon chips to alumina substrates. IEEE Trans. Compon. Packaging Manuf. Technol. **2011**, 1(12), 1983–1987.
7. Moran, B., Wu, F., Romanov, A.E., Mishra, U.K., Denbaars, S.P., Speck, J.S. Structural and morphological evolution of GaN grown by metalorganic chemical vapor deposition on SiC substrates using an AlN initial layer. J. Cryst. Growth 2004, 273, 38–47.
8. Gerthoffer, A., Poulain, C., Roux, F., Emieux, F., Grenet, L., Perraud, S. CIGS solar cells on ultra-thin glass substrates: Determination of mechanical properties by nanoindentation and application to bending-induced strain calculation. Solar Energy Mater. Solar Cells **2017**, 166, 254–261.
9. Seo, K., Nam, K.H., Lee, S., Han, H. Low stress polyimide/silica nanocomposites as dielectrics for wafer level chip scale packaging. Mater. Lett. **2020**, 263, 127204.
10. Liu, Y., Wang, Y., Wu, D. Synthetic strategies for highly transparent and colorless polyimide film. J. Appl. Polym. Sci. **2022**, 139, e52604.
11. Yang, Y., Jung, Y., Cho, M.D., Lee, S.G., Kwon, S. Transient color changes in oxidative-stable fluorinated polyimide film for flexible display substrates. RSC Adv. **2015**, 5, 57339–57345.
12. Zhi, X., Jiang, G., Zhang, Y., Jia, Y., Wu, L., An, Y., Liu, J., Liu, Y. Preparation and properties of colorless and transparent semi-alicyclic polyimide films with enhanced hightemperature dimensional stability via incorporation of alkyl-substituted benzanilide units. J. Appl. Polym. Sci. **2022**, 139, 51544.
13. Wang, Y., Liu, X., Shen, J., Zhao, J., Tu, G. Synthesis of a novel rigid semi-alicyclic dianhydride and its copolymerized transparent polyimide films' properties. Polymers **2022**, 14(19), 4132.
14. Wei, X.Y., He, Z.B., Yuan, S.Q., Wu, H., Zhi, X.X., Zhang, Y., Chen, S.J., Liu, J.G. Enhancement of ultraviolet light resistance of colorless and transparent semi-alicyclic polyimide nanocomposite films via the incorporation of hindered amine light stabilizers for potential applications in flexible optoelectronics. Polymers **2022**, 14(6), 1091.
15. Yan, X., Dai, F., Ke, Z., Yan, K., Chen, C., Qian, G., Li, H. Synthesis of colorless polyimides with high T_g from asymmetric twisted benzimidazole diamines. Eur. Polym. J. **2022**, 164, 110975.
16. Sawada, R., Ando, S. Colorless, low dielectric, and optically active semialicyclic polyimides incorporating a biobased isosorbide moiety in the main chain. Macromolecules **2022**, 55, 6787–6800.
17. Ozawa, H., Ishiguro, E., Kyoya, Y., Kikuchi, Y., Matsumoto, T. Colorless polyimides derived from an alicyclic tetracarboxylic dianhydride, CpODA. Polymers **2021**, 13, 2824.
18. Hasegawa, M., Sato, H., Hishino, K., Arao, Y. Ishii, J. Colorless polyimides derived from octahydro-2,3,6,7-anthracenetetracarboxylic dianhydride. Polymers **2023**, 3, 175–199.
19. Hasegawa, M., Horiuchi, M., Kumakura, K., Koyama, J. Colorless polyimides with low coefficient of thermal expansion derived from alkyl-substituted cyclobutanetetracarboxylic dianhydrides. Polym. Int. 2014, 63, 486-500.
20. Hasegawa, M., Ichikawa, K., Takahashi, S., Ishii, J. Solution-processable colorless polyimides derived from hydrogenated pyromellitic dianhydride: Strategies to reduce the coefficients of thermal expansion by maximizing the spontaneous chain orientation behavior during solution casting. Polymers 2022, 14, 1131.
21. Xia, X., He, X., Zhang, S., Zheng, F., Lu, Q. Short-side-chain regulation of colorless and transparent polyamide-imides for flexible transparent displays. Eur. Polym. J. 2023, 191, 112030.
22. Zhang, Y., Zhou, Y., Wang, Z., Yan, J. Colorless poly(amide-imide) copolymers for flexible display applications. J. Appl. Polym. Sci. **2022**, 139, e53082.
23. Jiang, G., Wang, D., Du, H., Wu, X., Zhang, Y., Tan, Y., Wu, L., Liu, J., Zhang, X. Reduced coefficients of linear thermal expansion of colorless and transparent semi-alicyclic polyimide films via incorporation of rigid-rod amide moiety: Preparation and properties. Polymers **2020**, 12, 413.
24. Hasegawa M, Watanabe Y, Ishii J. Solution-processable colorless polyimides with ultralow coefficients of thermal expansion for optoelectronic applications. Polym. Int. 2016, 65, 1063–1073.
25. Ren, X., Wang, H., Du, X., Qi, H., Pan, Z., Wang, X., Dai, S., Yang, C., Liu, J. Synthesis and properties of optically transparent fluoro-containing polyimide films with reduced linear coefficients of thermal xxpansion from organo-soluble resins derived from aromatic diamine with benzanilide units. Materials **2022**, 15, 6346.
26. Xia, X., Zhang, S., He, X., Zheng, F., Lu, Q. Molecular necklace strategy for enhancing modulus and toughness of colorless transparent polyimides for cover window application. Polymer **2022**, 259, 125358.
27. Morikawa, A., Iyoku, Y., Kakimoto, M., Imai, Y. Preparation of a new class of polyimide-silica hybrid films by sol-gel process. Polym. J. **1992**, 24(1), 107–113.
28. Bae, W.J., Kovalev, M.K., Kalinina, F., Kim, M., Cho, C. Towards colorless polyimide/silica hybrids for flexible substrates. Polymer 2016, 105, 124–132.
29. Moon, K.H., Chae, B., Kim, K.S., Lee, S.W., Jung, Y.M. Preparation and characterization of transparent polyimide-silica composite films using polyimide with carboxylic acid groups. Polymers 2019, 11(3), 489.

 doi:10.20944/preprints202306.1424.v1

30. Wang, Y.W., Chen, W.C. Synthesis, properties, and anti-reflective applications of new colorless polyimide-inorganic hybrid optical materials. Compo. Sci. Technol. 2010, 70, 769–775.